Proposition and Experiment of a Sliding Angle Self-Tuning Wave Energy Converter

Hoang-Thinh DO[a,b], Quang-Truong DINH[c], Minh-Tri NGUYEN[d], Cong-Binh PHAN[e], Tri-Dung DANG[d], Seyoung LEE[d], Hyung-Gyu PARK[e] and Kyoung-Kwan AHN[e*]

Abstract — The hydraulic power-take-off mechanism (HPTO) is one of the most popular methods in wave energy converters (WECs). However, the conventional HPTO with a fixed direction motion has some drawbacks which limit its power capture capability. This paper proposes a *sliding angle self-tuning wave energy converter (SASTWEC)* to find the optimal sliding angle automatically, with the purpose of increasing the power capture capability and energy efficiency. Furthermore, a small scale WEC test rig was fabricated and a wave making source has been employed to verify the sliding angle performance and efficiency of the proposed system throughout experiments.

[a] Division of Computational Mechatronics, Institute for Computational Science, Ton Duc Thang University, Ho Chi Minh City, Vietnam.

[b] Faculty of Electrical & Electronics Engineering, Ton Duc Thang University, Ho Chi Minh City, Vietnam.

[c] International Digital laboratory (IDL), WMG, University of Warwick, CV4 7AL, United Kingdom.

[d] Graduate School of Mechanical and Automotive Engineering, University of Ulsan, Ulsan 680-749, Korea.

[e] School of Mechanical and Automotive Engineering, University of Ulsan, Ulsan 680-749, Korea.

[*]Corresponding author. Tel: +82-52-259-2282; fax: +82-52-259-1680

E-mail: kkahn@ulsan.ac.kr (K. K. AHN), dohoangthinh@tdt.edu.vn (H.T. DO).

Index Terms **— hydrostatic transmission, wave energy converter, self-tuning, floating buoy, power-take-off mechanism**

1. Introduction

The increased energy demand and environmental pollution push people and organizations to find sustainable energy sources and reduce exhaust emissions. An urgent need exists to harvest energy from renewable sources such as wave energy. Many studies have been conducted in the field of wave energy and various wave energy conversion systems or wave energy converters (WECs) are currently being developed, such as overtopping devices (e.g., the Wave Dragon), attenuators (Pelamis), and point absorbers (WaveBob, OPT PowerBuoy), as noted in [1]. the main principle of WECs is to convert wave energy into high-pressure hydraulic on, which is used to drive a hydraulic motor coaxially connected to an electric generator. The mechanism by which energy is transferred from waves to the WEC, and subsequently or directly into a useful form is called a hydraulic power take-off mechanism, generally known as the power take-off (PTO). The Pelamis WEC, using an active control of PTO to maximize the absorbed power throughout a range of sea-states was presented in [2]. A seabed-mounted bottom-hinged flap-type wave energy converter was proposed and designed in [3] increases the capture factor width and wave frequency. While this design appears to be effective, when it is mounted on the sea bottom, several problems appear such as difficulty in maintenance, corrosion by sea water, and oil leakage pollution. In [4], a flap-type wave maker and the submerged cylinder WEC is proposed and modeled based on the complete solution of the Navier-Stokes equations to predict the behavior of the submerged cylinder WEC subjected to highly nonlinear incident waves. The numerical results and the analytics are observed in a good agreement, and the

maximum efficiency point moves toward higher wave frequencies with increasing the wave height. One of the simplest and most popular wave energy converters is the point absorber type, mentioned in [5] and [6]. However, wave energy is absorbed in only one direction, either vertical or horizontal. Therefore, this limits the total efficiency of the converter. Evans in [7] proposed a wave-power absorption device which can absorb both the horizontal and vertical force components. It is shown that theoretically 100% efficiency is possible in some cases. In [8], Heikkinen et al. proposed a new structure of cylindrical wave energy converters oscillating in two modes. This approach can absorb energy in two directions to improve the total efficiency. However, similar to the seabed-mounted bottom-hinged wave energy converter in [3], it still has some drawbacks, such as difficulty in maintenance, corrosion, and oil leakage. To determine the cylindrical wave coefficients of any wave field from a known circular-cylindrical section, four types of WECs were used: a heaving point absorber, a surging point absorber, a terminator, and an attenuator in [9]. According to Folley in [10], there exists a significant direction or sector in which wave energy is the most energetic. Therefore, a wave energy converter with a predefined direction is more effective than the conventional WEC, such as a vertical linear motion WEC.

Moreover, to overcome the drawbacks of the above wave energy converters and enhance the total efficiency, a sliding angle self-tuning wave energy converter (SAST-WEC) is proposed in this paper. The optimal sliding angle varies with the wave condition. In the proposed system, SAST-WEC can calculate the optimal sliding angle and self-tune the sliding angle to enhance the output power and efficiency. A small-scale SAST-WEC test rig is fabricated to verify the effect of the proposed method. An experiment was carried out in three wave conditions for monitoring the performance of SAST-WEC, although the wave condition changes in reality. This work is the next step of the research has been presented in [11].

The remainder of this paper is organized as follows. Section 2 describes the wave making tank and the test rig of the SAST-WEC, section 3 presents the mathematical model of SAST-WEC, and section 4 shows the experiments and analysis of the experimental results. Finally, conclusions and future works are presented in section 5.

2. Description of wave making tank and adjustable sliding angle wave energy converter

2.1 Wave making tank

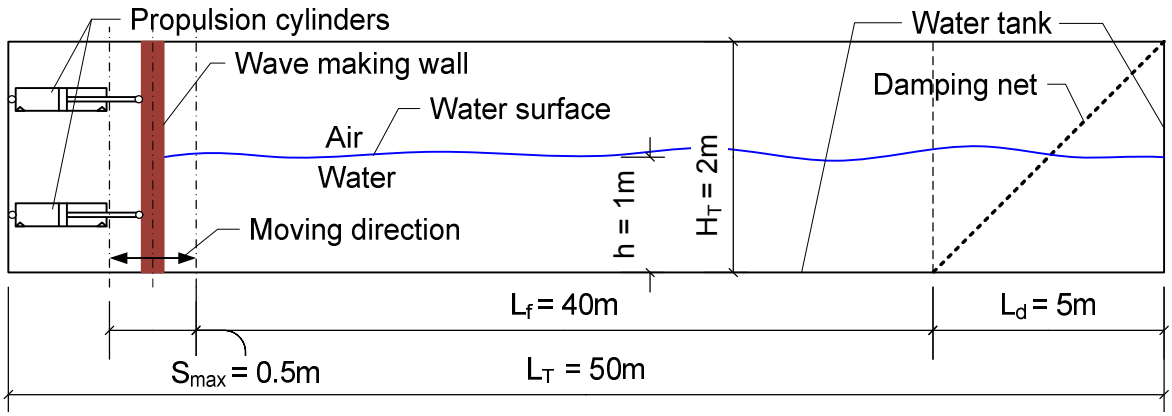

Fig. 1 Schematic diagram of wave making tank

To carry out the experiment, a wave making tank with an adjustable amplitude and frequency is employed, as shown in Fig. 1. The wave making tank includes a wave making wall moved by propulsion hydraulic cylinders, placed in a water tank. A slope damping net attached at the opposite side of the wave making wall eliminates the reflex wave to avoid unexpected noise. The motion of the wave making wall and cylinders are set up and controlled by a computer and sensors to achieve the exact wave amplitude and frequency. The working principle of the wave making tank in this research is similar to the *wave maker* described in [12].

2.2 Self-tuning sliding angle wave energy converter

The sea wave has the vertical oscillation and the horizontal propagation. These two motions bring the sea water and create the hydrodynamic forces. The vertical oscillation creates the heave force and the horizontal propagation creates the surge force. The heave force and the surge force will be shown in Eq. (4) and Eq. (14) of the subsection 3.2. The conventional PTO with vertical oscillation can absorb the heave force only, whereas the proposed PTO can absorb both the heave force and the surge force, as shown in Fig. 2. The force F_w is the resultant of F_{heav} and F_{surg}. Therefore, the force F_w is obviously greater than the heave force F_{heav} only.

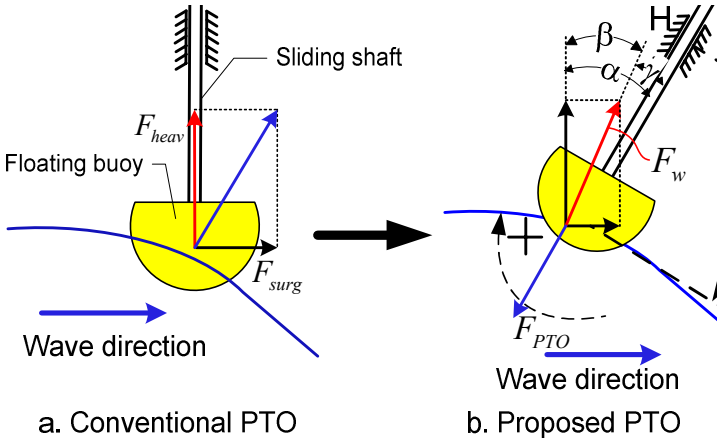

Fig. 2 Force comparison between the conventional PTO and the proposed PTO

In addition, the buoy's stroke of the proposed PTO is longer than the buoy's stroke of the conventional PTO. With the same wave amplitude and frequency, when moving in the slope angle from the wave trough to the wave crest, due to the buoy's stroke is longer than moving a vertical direction. As illustrated in Fig. 3, the buoy's stroke Δ in the slope angle in longer than the buoy's stroke Ψ of the conventional PTO.

The stronger force gives the higher pressure, and the longer stroke gives the higher flow rate at the cylinder. Hydraulic power generated at the cylinder is calculated by the product of fluid

pressure and fluid flow rate. Hence, the hydraulic power of the proposed PTO is higher. The effects of non-vertical linear motions the investigation of optimal sliding angle was presented in [11].

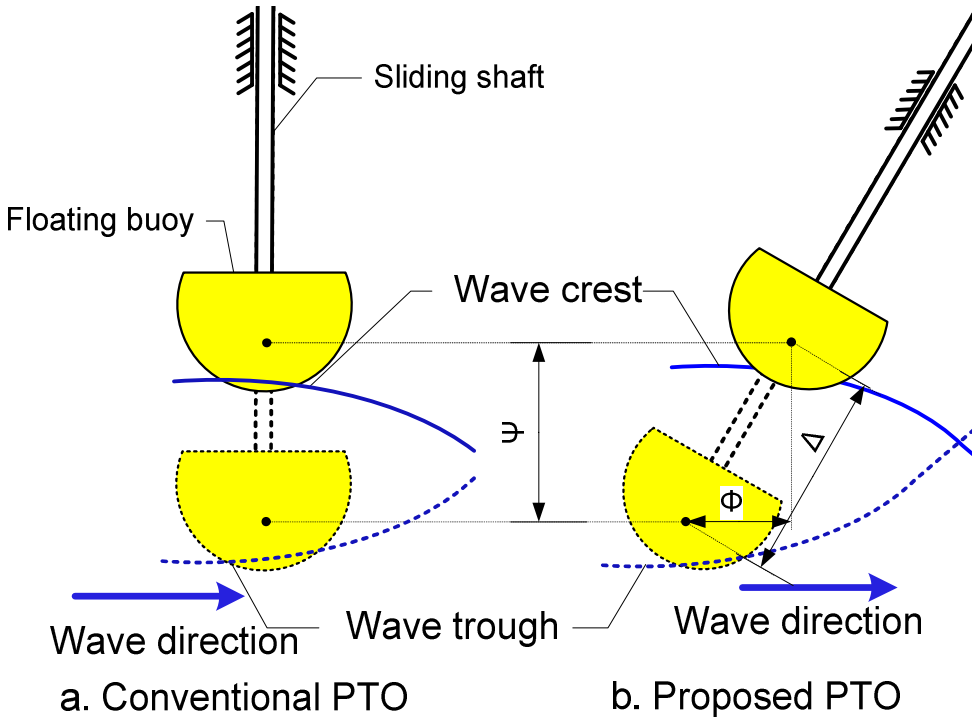

Fig. 3 Buoy's stroke comparison between the conventional PTO and the proposed PTO

The test rig of SAST-WEC includes two components, as shown in Fig. 4: the HPTO and the hydraulic transmission. In the HPTO, a floating buoy attached to a sliding shaft can be moved by a wave, as shown in the upper photograph of Fig. 4. As revealed in [13], a semi-sphere floating buoy is preferred in the test rig. The sliding shaft with a set of 4 load-cells, is supported by rollers, to ensure the shaft moves with low friction in a linear direction. The set of 4 load-cells can collect data on the vertical and horizontal forces by exerting waves on the floating buoy. The sliding shaft connects to a hydraulic cylinder which functions as a hydraulic

pump to pressurize the hydraulic fluid. The sliding angle adjustment is carried out using a rotation mechanism with an electric actuator and a potential meter. The sliding angle control signal is given by a PID closed-loop controller from a computer.

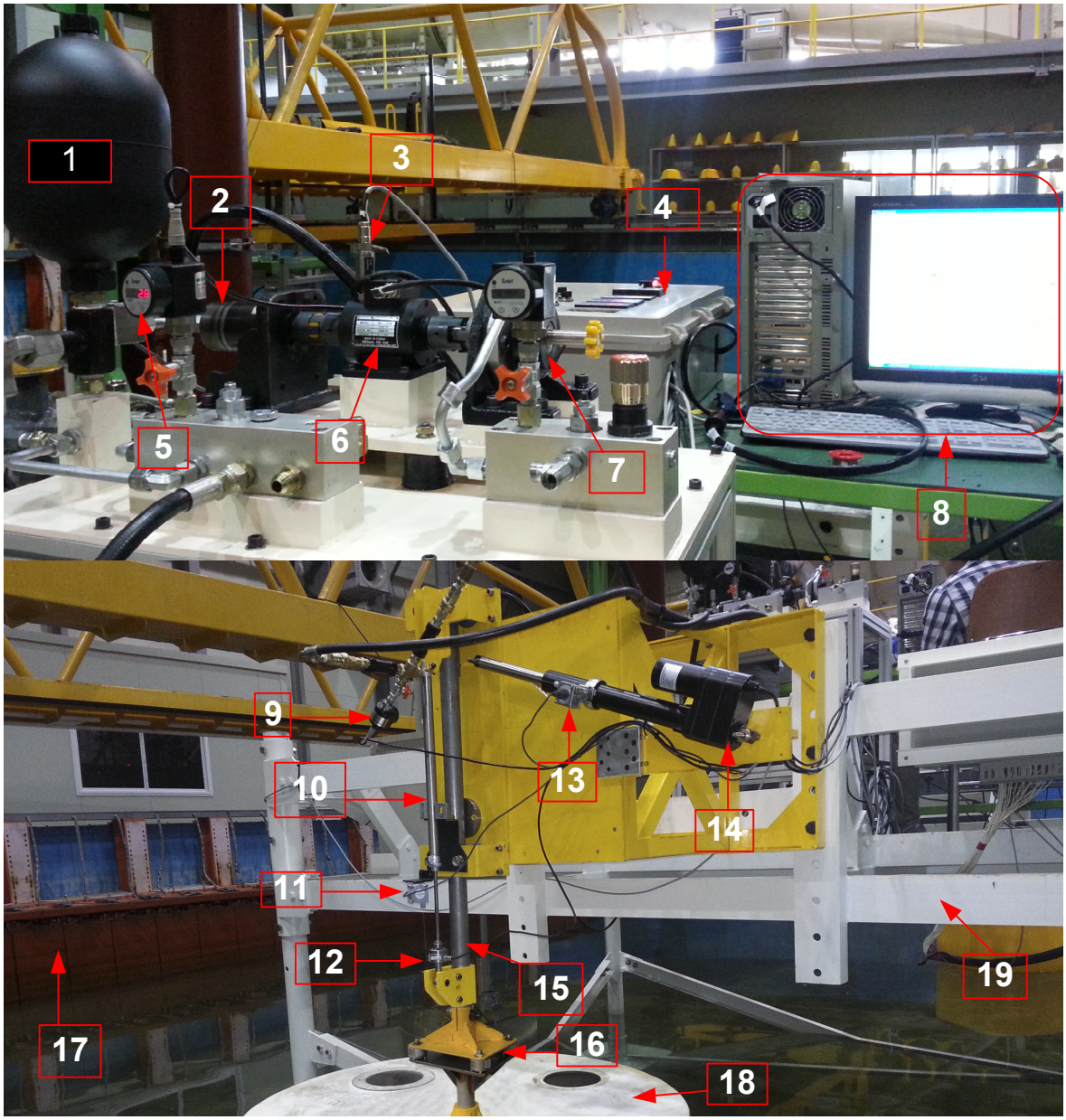

Fig. 4 SAST-WEC test rig

1- HPA; 2- Hydraulic motor; 3- Speed sensor; 4- Data acquisition and control box; 5- Pressure sensor 2; 6- Torque sensor; 7- 'Generator'-MR brake; 8- Computer; 9- Pressure sensor 1; 10- Cylinder; 11- Potential meter; 12- Loadcell; 13- Potential meter for angle adjustment; 14- Actuator for angle adjustment; 15- Moving shaft; 16- 4 loadcell set; 17- Wave making wall; 18- Floating buoy; 19- Frame

The hydrostatic PTO is supported by a frame and connected by hydraulic hoses. A low-pressure hose carries the low-pressure fluid from the tank to the hydraulic cylinder, while a high-pressure hose passes the pressurized fluid from the cylinder to the high-pressure accumulator and hydraulic motor of the hydraulic transmission as shown in the lower photograph of Fig. 4.

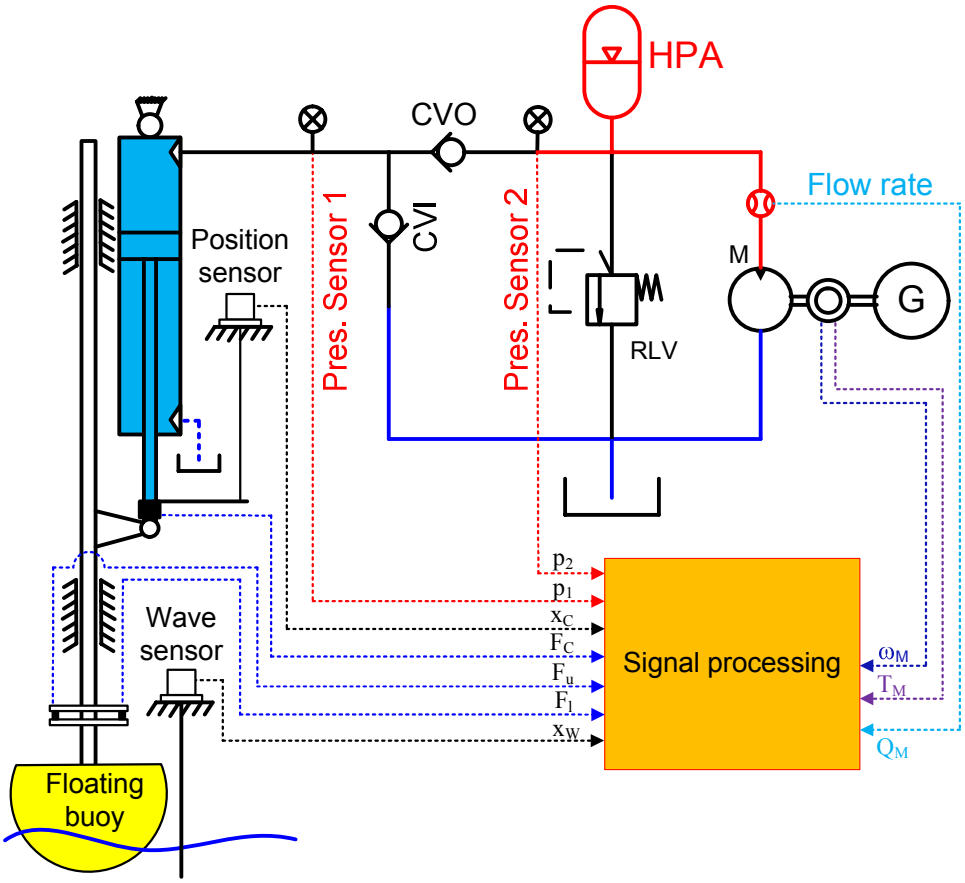

Fig. 5 Hydraulic circuit of SAST-WEC

The hydraulic circuit of SAST-WEC is shown in Fig. 5. When the cylinder is extended, fluid is sucked from the tank to the full bore chamber of the cylinder. The CVI check valve allows low-pressure fluid from the low-pressure hose to enter the cylinder but restricts entry of the

fluid in the opposite direction. When the cylinder is compressed, fluid in the full bore chamber is pressurized and pumped to the high-pressure accumulator (HPA). The CVO check valve allows the high-pressure fluid from the cylinder to the high-pressure hose to charge the HPA but restricts the fluid in the opposite direction. The hydraulic motor is driven by high-pressure fluid from the HPA. By employing HPA, the operating pressure is smoothened and the fluctuation of the hydraulic motor velocity is reduced. The relief valve RLV1 releases pressure in the HPA to protect the hydraulic circuit if the operating pressure becomes too high. A Magnetorheological (MR) brake is used to simulate the load of a generator. A torque and speed sensor are placed between the hydraulic motor and the "generator" (herein MR brake) for output power calculation. The parameters of the components of SAST-WEC are shown in Table 1.

Table 1. Parameters of SAST-WEC

Parameter		**Symbol**	**Value**
Cylinder	Bore diameter	D	25mm
	Rod diameter	d	12mm
	Length	l	0.5m
Accumulator	Volume	V_0	3L
	Pre-charged press.	p_0	5bar
Hydraulic motor	Displacement	D_m	12.5cc/rev

Data of the wave, floating buoy motion, buoyant force, the pressure of cylinder and accumulator, flow rate of the hydraulic motor, output torque, and speed are collected from the corresponding sensors and sent to an industrial computer via a data acquisition card (NI 6289 PCI card). The Matlab Simulink program is built for sliding angle control and data processing.

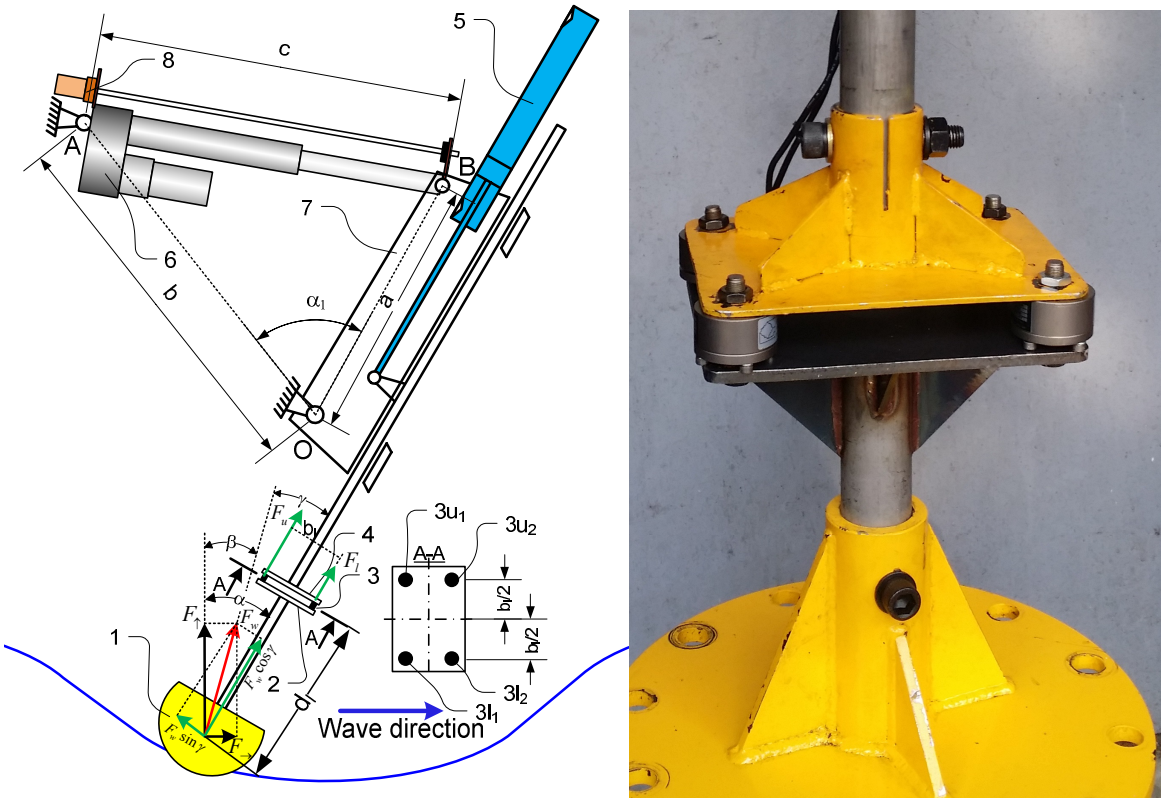

Fig. 6 The optimal sliding angle approximation shaft

Fig. 6a Schematic diagram of the optimal sliding angle approximation shaft; Fig. 6b. The optimal sliding angle approximation shaft on real test rig1- Floating buoy; 2- lower plate; 3- load-cells: $3u_{1,2}$ – upper load-cell, $3l_{1,2}$ – lower load-cell; 4- upper plate; 5- cylinder; 6- electric actuator; 7- swash plate; 8- linear position sensor.

3.Mathematical modeling of the self-tuning sliding angle wave energy converter

3. 1 Wave Model

An irregular ocean wave can be represented as the superposition of single waves as described by the Pierson-Moskowitz spectrum from [14], as in Fig. 7. The irregular wave spectrum is represented by the significant wave height H_s and the peak wave period T_p.

An irregular wave can be generated as a sum of the wave components as discussed in [15]:

$$Y(t) = \sum_{i=1}^{n} \sqrt{2S_A(f_i)\Delta f}\,\sin\left(2\pi f_i t + \varphi_{rand,i}\right) \quad (1)$$

where $Y(t)$ is the irregular wave displacement; $S_A(f_i)$ is the spectral density of the represented sea states; Δf is the increment of wave frequency; and f_i and $\varphi_{rand,i}$ are the frequency and random phases of each component, respectively.

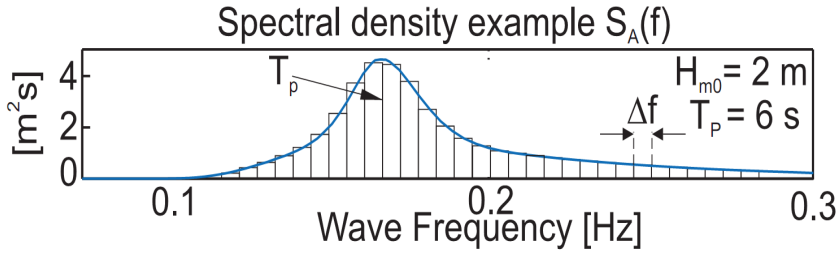

Fig. 7 Wave spectra for sea states

3. 2 Hydrodynamic model of a floating buoy

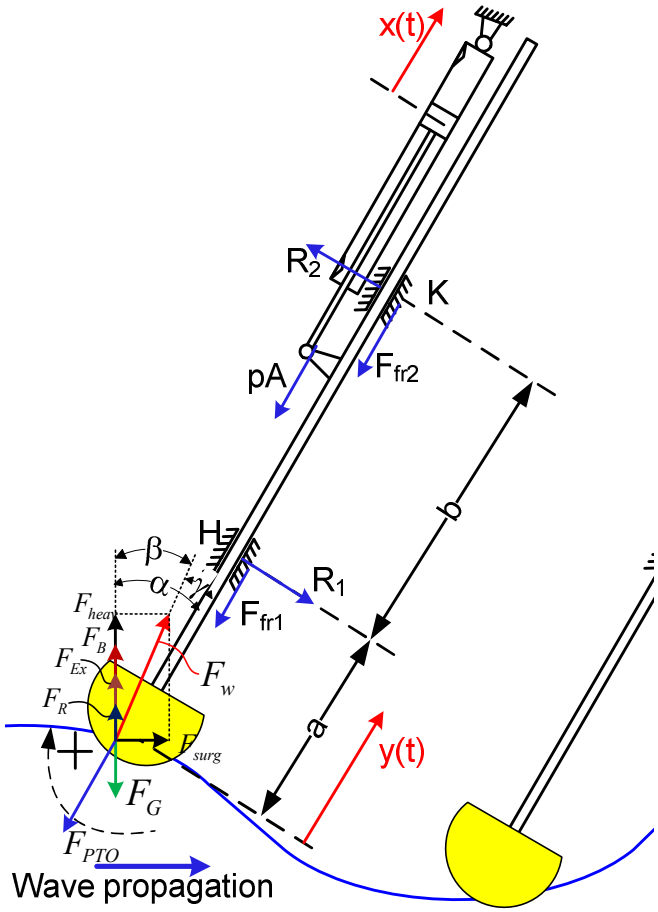

Fig. 8 Detail view and force analysis of PTO

The motion of a floating buoy can be described using the following equation:

$$\left(m_b + m_s\right)\ddot{y}\left(t\right) = F_w \cos\gamma - F_{PTO} \tag{2}$$

where m_b and m_s are the mass of the floating buoy and the mass of the sliding shaft, respectively, $y(t)$ is the displacement of the floating buoy, F_{PTO} is the force to move the cylinder piston in order to generate a high-pressure fluid, and F_w is the resultant force of the wave on the floating buoy. From Fig. 8 F_w is included in the vertical component or heaving force F_{heav} and horizontal component or surge force F_{surg}:

$$F_w = F_{heav} + F_{surg} \tag{3}$$

According to [16], the vertical force exerting on the floating buoy can be represented as a superposition of three components: the hydrostatics force, the excitation force applied by an incoming regular wave to a fixed float, and the radiation force experienced by an oscillating float, which is the sum of the forces created by the motion of the other buoys floating on the water. The heaving force from the wave is defined as:

$$F_{heav} = F_B + F_{Ex} + F_R - F_G \tag{4}$$

Here, F_B is the buoyant force, F_{Ex} is the excitation force, and F_R is the radiation force, produced by an oscillating body creating waves on a calm sea.

The buoyant force F_B is calculated as:

$$F_B = \rho g V_s \tag{5}$$

Here, ρ is the density of water, g is the gravitational acceleration, and V_s is the volume of the floating buoy that is below the water surface, as shown in Fig. 9, defined as:

$$V_s = \begin{cases} \frac{\pi}{3}(3R - z)z^2, & 0 < z \le R \\ \frac{2\pi}{3}R^3 + \pi R^2(z - R), & R < z \le R + h \end{cases} \tag{6}$$

where z is the submerged level of the floating buoy.

The excitation force F_{Ex} is expressed as shown in [18]:

$$F_{EX} = f_3 \frac{H}{2} \sin \omega_w t \tag{7}$$

Where f_3 is the excitation force coefficient, which is dependent on the body's shape, discussed in [17], and H is the wave height (from peak to peak).

$$\Gamma(\omega_w) = \sqrt{\frac{2g^3 \rho B(\omega_w)}{\omega_w^3}} \tag{8}$$

The coefficient $B(\omega_w)$ depends on the wave frequency.

The radiation force is expressed as:

$$F_R = -(m_{Ad}\ddot{y} + b_{rad}\dot{y}) \tag{9}$$

where b_{rad} is the impulse response function describing the hydrodynamic damping. From Newton's viscosity law and some manipulations, we can get the hydrodynamic damping coefficient b_{Ad} in the water tank as:

$$b_{Ad} = \mu \frac{A_s}{e} \tag{10}$$

where μ is the viscous dynamic viscosity of water, shown in Table 2; A_s is the area of the floating buoy in contact with the water, calculated as:

$$A_s = \pi \left[\left\{ a\sin\left(\frac{R-z}{R} \right) \right\}^2 + z^2 \right] \tag{11}$$

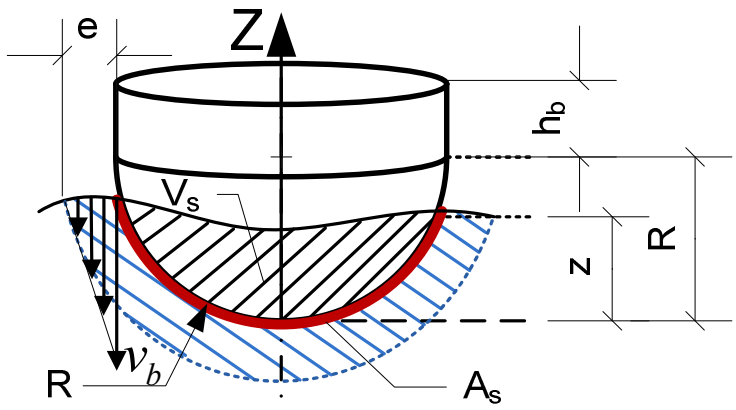

Fig. 9 Buoy shape and water level

The term m_{Ad} represents the "added mass"; this term is included to account for the fact that, when a float oscillates, it appears to have a greater mass due to the water that is displaced along with it, as shown in [18]. m_{Ad} is calculated as:

$$m_{Ad} = \rho V_s \tag{12}$$

F_G is the gravity force, calculated as:

$$F_G = (m_b + m_s)g \tag{13}$$

The surge force from a wave is called as drag force, and is defined as:

$$F_{surg} = \frac{1}{2}\rho v^2 C_D A_{bh} \tag{14}$$

where v is the wave velocity, C_D is the drag coefficient and A_{bh} is the wet cross-section of the buoy on a plane perpendicular to the direction of the wave:

$$A_{bh} = \begin{cases} R^2\left[\arcsin\left(\frac{z-R}{R}\right)\right] + \frac{\sin 2\left[\arcsin\left(\frac{z-R}{R}\right)\right]}{2} + \frac{\pi}{2}, & 0 < z \le R \\ \frac{\pi}{2}R^2 + 2R(z-R), & R < z \le R + h_b \end{cases} \tag{15}$$

3. 3 Model of hydraulic cylinder

In this approach, a cylinder has been employed as a hydraulic pump to convert the kinetic energy of a floating buoy into the potential energy stored in the HPA. We define *x(t)* as the *x*-coordinate of the piston. The cylinder rod is fixed to the floating buoy, so:

$$\dot{x}(t) = \dot{y}(t) \tag{16}$$

As the piston of the cylinder is in a moving condition, the continuity equation of the bore chamber is:

$$\frac{dp_1}{dt} = \frac{\beta}{A_p L_0 - A_p x_i}\left(A_p \dot{x} + Q_{CVI} - Q_{CVO}\right) \tag{17}$$

where, β is the bulk modulus of oil in Pa, $A_p L_0$ is the initial volume of the bore chamber, and A_P is the piston area in m^2:

$$A_p = \pi D^2 / 4 \tag{18}$$

D is the bore diameter.

Q_{CVI} is the input flow rate from the tank to the cylinder via the *CVI* check valve:

$$Q_{CVI} = \begin{cases} C_d A_{CVI} \sqrt{2|p_t - p_1| / \rho}, & if\ p_t > p_1 \\ 0, & else \end{cases} \tag{19}$$

Q_{CVO} is the output flow rate from the cylinder to the HPA via *CVO* check valve:

$$Q_{CVO} = \begin{cases} C_d A_{CVO} \sqrt{2|p_1 - p_2| / \rho}, & if\ p_1 > p_2 \\ 0, & else \end{cases} \tag{20}$$

p_1 is the pressure at the cylinder port defined by Eq. (17), p_2 is the pressure of the fluid in the high-pressure hose, C_d is the discharge coefficient, cylinder friction $C_d = 0.7$ for hydraulic oil, and A_{CVO} is the cross-section of the *CVO* check valve.

The cylinder force is calculated as:

$$F_{PTOi} = \Delta p_{1t} A_p + F_{fric} \tag{21}$$

Where:

$$\Delta p_{1t} = p_1 - p_t \tag{22}$$

p_t is considered to be the pressure in the tank.

F_{fri} is the friction force of the cylinder, defined as [15]:

$$F_{fric} = \left|\Delta p_{1t} A_p\right|\left(1 - \eta_c\right) \tag{23}$$

The cylinder friction F_{fric} is defined such that the cylinder has a friction coefficient η_c= 0.98.

3. 4 Modeling and calculation of the HPA

A bladder accumulator, which is filled with nitrogen gas, is employed in the proposed system. According to [19], the nitrogen gas is assumed to compress and expand based on the adiabatic gas law:

$$pV^n = p_0 V_0^n = p_{\max} V_{\min}^n \tag{24}$$

Then the fluid volume in the HPA is then derived as:

$$V_{HPA} = \begin{cases} 0, & if\ p_2 \le p_0 \\ V_0 \left(1 - p_0 / p_2\right)^{1/n}, & else \end{cases} \tag{25}$$

where V_0 is the initial volume of the HPA, p_0 is the pre-charged pressure, p_2 is the pressure of the high-pressure hose and n is the adiabatic coefficient.

The energy that can be absorbed by the HPA is calculated as:

$$E = V_0 p_0^{1/n} \left[p_{\max}^{(n-1)/n} - p_0^{(n-1)/n} \right] / (n-1) \tag{26}$$

The optimal pre-charged pressure for the maximum energy capacity of HPA is given by:

$$p_0 = n^{-n/(n-1)} p_{\max} \tag{27}$$

and the maximum energy that is stored in HPA is given by:

$$E_{\max} = p_{\max} V_0 / n^{n/(n-1)} \tag{28}$$

The volume of the HPA can then be derived as:

$$V_0 = E_{\max} n^{n/(n-1)} / p_{\max} \tag{29}$$

3. 5 Model of connecting hose

Using the flow continuity equation, the pressure in the high-pressure hose is expressed as:

$$\frac{dp_2}{dt}=\frac{\beta}{V_h}\left(Q_{CVO}-Q_{HPA}-Q_r-Q_m\right) \tag{30}$$

Where:

β is the fluid bulk modulus;

V_h is the volume of the hoses;

Q_{CVO} represents the flow rate through the *CVO* check valves, as formulated in Eq. (20);

Q_{HPA} is the flow rate into the HPA, derived based on Eq. (25) as:

$$Q_{HPA}=\dot{V}_{HPA}=\begin{cases}0, \ if \ p_h \le p_0 \\ \dfrac{1}{n}V_0\left(1-\dfrac{p_0}{p_h}\right)^{\frac{1-n}{n}}\dfrac{p_0\dot{p}_h}{p_h^2}, \ else\end{cases} \tag{31}$$

and Q_r is the flow rate through the relief valve RLV.

According to [20], Q_r can be expressed as:

$$Q_r=\begin{cases}0, & if \ \Delta p_{2t} \le \Delta p_{set} \\ C_d A_v\sqrt{2\Delta p_{2t}/\rho}, & if \ \Delta p_{2t} \ge \Delta p_{set}\end{cases} \tag{32}$$

where, A_v is the valve throttling area in m^2.

Q_m is the actual flow rate of the hydraulic motor as shown in Eq. (37), and Δp_{2t} is the pressure difference between the high-pressure hose and low-pressure hose, which is considered to be the pressure in the tank:

$$\Delta p_{2t}=p_2-p_t \tag{33}$$

3. 6 Model of the hydraulic motor

The ideal flow rate of the piston hydraulic motor is defined as:

$$Q_{mi}=\alpha D_{\max}\omega_M \tag{34}$$

where ω_M is the motor rotation speed.

The volumetric efficiency, mechanical efficiency, actual flow rate and actual output torque of the piston hydraulic motor are expressed in Eqs. (32), (33), (34), and (35), respectively.

$$\eta_{vM} = \alpha D_{\max} \omega_M / \left(\alpha D_{\max} \omega_M + Q_l \right) \tag{35}$$

$$\eta_{tM} = \left(\alpha_M D_{\max} \Delta p - T_{loss} \right) / \left(\alpha_M D_{\max} \Delta p \right) \tag{36}$$

$$Q_m = Q_{mi} / \eta_{vM} \tag{37}$$

$$T_m = \alpha_M \Delta p D_{\max} \eta_{tM} \tag{38}$$

Here, Q_l and T_l are the loss flow rate and the loss torque of the pump, respectively, as discussed in [21]; α_M, $D_{\max}$, Δp are the displacement ratio, the maximum displacement and the pressure difference between the two ports of the motor, respectively.

3. 7 Measurement of *sliding angle*

- Referring to Fig. 6 and the cosine function theorem, the angle α_1 is defined as:

$$\alpha_1 = a\cos\left(\frac{a^2 + b^2 - c^2}{2ab} \right) \tag{39}$$

- Adjust the sliding angle α to zero (vertical direction, $\alpha = 0$).

- Measure *a* and *b*, which are fixed values, and variable *c*= c_0 at $\alpha = 0$. Then, according to the cosine function theorem, α_0 is defined as:

$$\alpha_0 = a\cos\left(\frac{a^2 + b^2 - c_0^2}{2ab} \right) \tag{40}$$

Note that c_0 is the length of *c* at sliding angle $\alpha = 0$.

Herein, the sliding angle α can be calculated by measuring the distance c with the linear position sensor:

$$\alpha = \alpha_1 - \alpha_0 \tag{41}$$

To calculate the *optimal sliding angle* β , a set of 4 load-cells is installed on the sliding shaft, as shown in Figs. 4b. Assume that the forces measured by load-cells are F_{u1} and F_{u2} at two upper load-cells, and F_{l1} and F_{l2} at two lower load-cells. Then the compressing force is determined as:

$$\begin{cases} F_u = F_{u1} + F_{u2} \\ F_l = F_{l1} + F_{l2} \end{cases} \tag{42}$$

The moment and force equations on the buoy are derived as:

$$F_w \sin\gamma d_l = \left(F_u - F_l\right)\frac{b_l}{2} \tag{43}$$

$$F_w \cos\gamma = F_u + F_l \tag{44}$$

Then:

$$\gamma = a\tan\left(\frac{b_l}{2d_l}\frac{\left(F_u - F_l\right)}{\left(F_u + F_l\right)}\right) \tag{45}$$

Data of F_u & F_l are collected as average values only in the upward stroke of the floating buoy within the last 20 minutes. Hence, Eq. (45) is rewritten as:

$$\gamma = a\tan\left(\frac{b_l}{2d_l}\frac{\left(\overline{F}_u - \overline{F}_l\right)}{\left(\overline{F}_u + \overline{F}_l\right)}\right) \tag{46}$$

where $\overline{F}_u$ & $\overline{F}_l$ are the mean average values of F_u & F_l, respectively.

From Fig. 6a, the optimal sliding angle β is calculated as:

$$\beta = \alpha - \gamma \tag{47}$$

Tilt-sliding angle adjustment:

The PTO system is placed on a plate which can rotate around pin O as shown in Fig. 6. $\gamma_{\min}$, $\gamma_{\max}$ are the minimum and maximum angle difference, respectively, operated by the power take off mechanism. The hydraulic cylinder is used to adjust the tilt-sliding angle α. After calculating, α is compared to β and adjusted to ensure that the angle difference is smaller than the minimum value:

$$|\gamma| = |\beta - \alpha| \le \gamma_{\min} \tag{48}$$

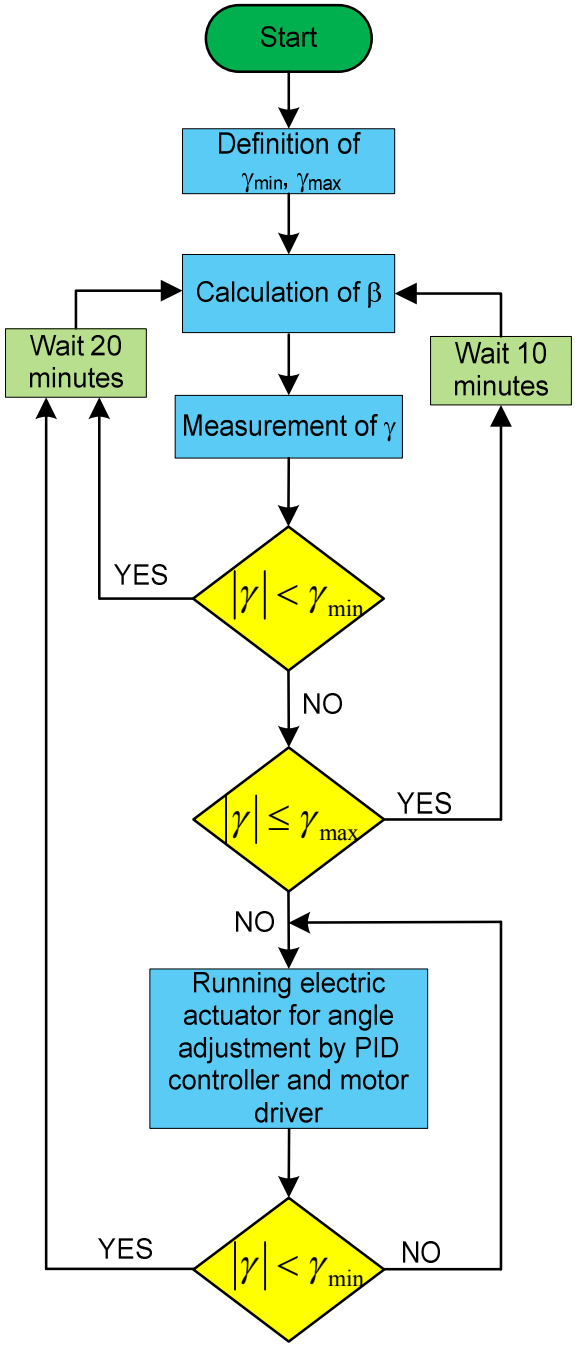

1

2 Fig. 10 Flowchart of the optimal angle control method for sliding mechanism

3 The flowchart of the optimal angle approximation and control method is shown in Fig. 10.

4 Eqs. (42) and (43) are used for the optimal sliding angle β approximation. If $|\gamma| < \gamma_{min}$, the

5 approximation will be repeated after 20 minutes; if $\gamma_{min} < |\gamma| < \gamma_{max}$, the approximation will be

repeated after 10 minutes; and if $|\gamma| \geq \gamma_{\max}$, the PID controller runs to extend or retract the cylinder into an optimal angle adjustment. If $\gamma < 0$, the cylinder retracts and if $\gamma > 0$, the cylinder extends. The controller will run until $\gamma < \gamma_{\min}$. After 20 minutes, the optimal angle approximation and controlling process will be repeated.

4. Experiment

4.1 Wave condition and energy flux

The wave conditions are designed and generated by the wave making tank. Wave conditions (WC) #1, #2, and #3 correspond to weak, medium, and strong waves, respectively. According to [22], the energy flux in 1 period for the shallow-water of the water tank is expressed as:

$$E = \frac{\rho g^{3/2} H^2 \sqrt{h} T b}{8} \tag{46}$$

Based on the parameters in Table 2, the results of energy flux for 1 period and 30s are given in Table 3.

Table 2 Parameters of floating buoy and water

Water density ρ [Kg/m^3]	**Dynamic viscosity μ [Pa.s]**	**Gravity g [m/s^2]**	**Buoy width b [m]**	**Water depth h [m]**
1000	0.001	9.81	0.9	1

Table 3 Wave energy flux

Wave condition	**Wave height H[m]**	**Wave period T[s]**	**Wave length λ [m]**	**Energy in 1 period [J]**	**Energy in 30s [J]**

#1	0.124	2.4	7.468	127.559	1594.486
#2	0.151	2.8	8.991	220.682	2364.456
#3	0.205	1.8	5.145	261.478	4357.978

1

2 **4.2 Simulation of the proposed wave energy converter**

3 Simulation is done with parameters the same as the real test rig, in the case of vertical linear
4 motion, wave condition # 3 and without sliding angle control. Only the simulation result and
5 experimental result of the input/output power and input/output energy is illustrated on Fig. 11
6 for comparison. Although the input power varies in a wide range from 0 to 350W, but by the
7 effect of the accumulator HPA, the output power is stable around 36W. After 30s, the input and
8 output energy of the simulation are calculated as 1659.6J and 1109.6J, respectively, while the
9 input and output energy of the experiment are calculated as 1594.9J and 976.4J. The
10 hydraulic efficiency of the WEC, which is the ratio of the output and the input energy, is 66.8%
11 in the simulation and 61.2% in the experiment. The total efficiency is defined by the ratio of the
12 output energy and 'Energy in 30s' as shown in Table 4. Then the overall efficiency is
13 calculated as 25.4% in the simulation and 22.4% in the experiment. The simulation and
14 experimental results are not exactly the same; however, they are in quite agreement. The
15 detailed simulation and experimental result comparison have been presented in [11].

16

17

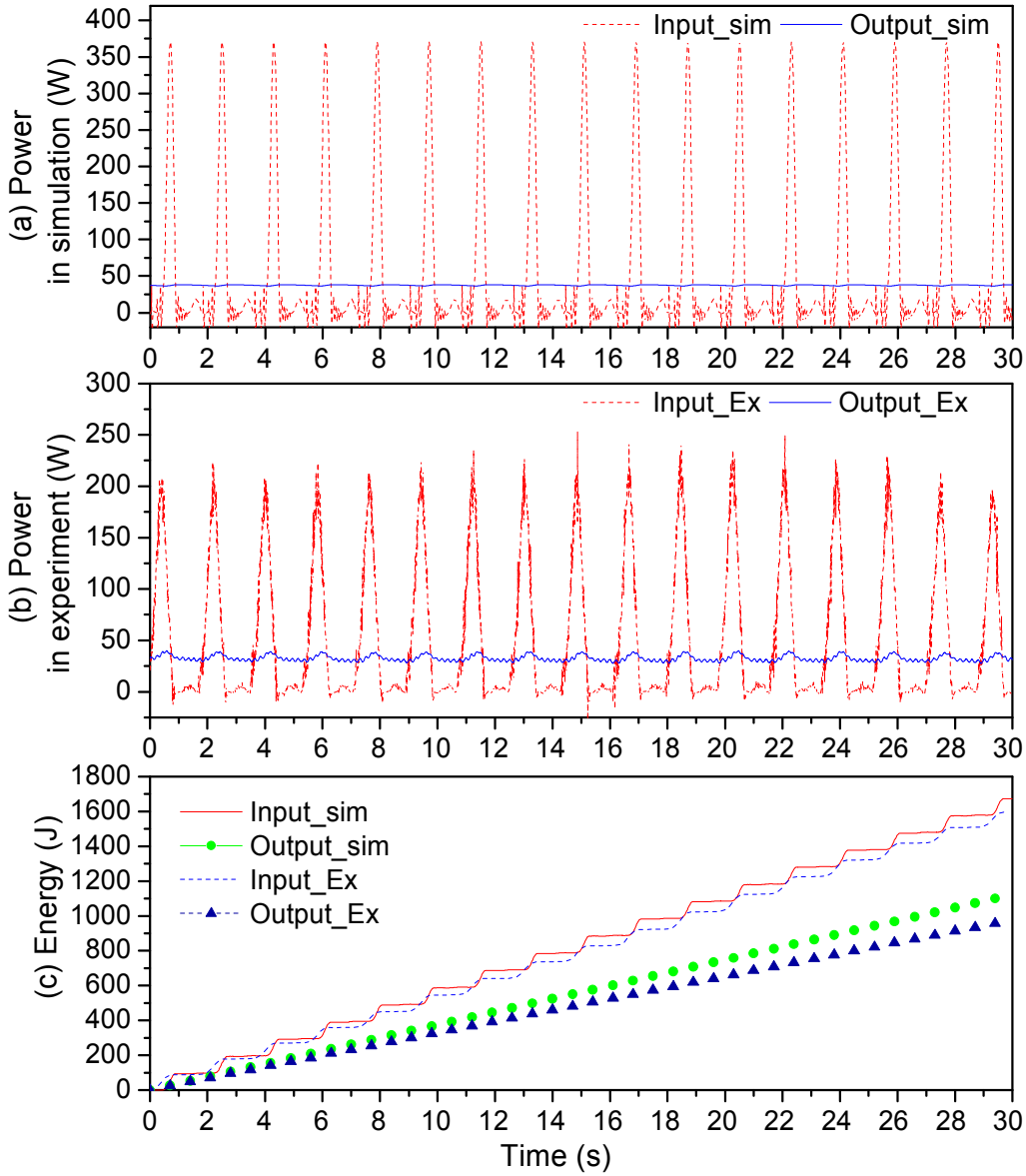

Fig. 11 Simulation and experimental results of input/output power and input/output energy in case of vertical linear motion and wave condition No. 3

4.3 Performance of the self-tuning sliding angle wave energy converter

Experiments are performed in three wave conditions #1, #2, and #3, corresponding to weak, normal and strong, respectively. The optimal sliding angle is calculated using Eq. (47) and the force data from the 4 load-cell set, as shown in Fig. 12. The last value of the calculated optimal sliding angle (dash curve) of each 30s is updated to the reference sliding angle (dot curve) in

1 the next 30s. In the flowchart shown in Fig. 10, the ‘angle sampling time’ or approximation
2 time is 20 minutes or 10 minutes upon the value of $|\gamma|$ for real wave application. Within the
3 limits of the experiments, the ‘angle sampling time’ is shorter (30s), because the wave
4 condition can be changed easily and quickly by control the wave making tank.
5 Initially, the reference sliding angle is given arbitrarily: 0^0 at WC #1, 5^0 at WC #2, and 7^0 at
6 WC #3. After the first ‘angle sampling time’, 30s, the reference sliding angle is updated by the
7 last value of the calculated optimal sliding angle of the previous 30s. The last value of the
8 calculated optimal sliding angle is also the average value of the optimal sliding angle in 30s.
9 The response sliding angle (solid curve) can successfully track the reference sliding angle by
10 the PID controller and electric actuator. Because of the clearance in fabrication, the graph of
11 the response sliding angle oscillates around the reference sliding angle with the frequency of
12 the wave. However, in a constant wave condition, the response sliding angle will convex to the
13 optimal sliding angle.
14

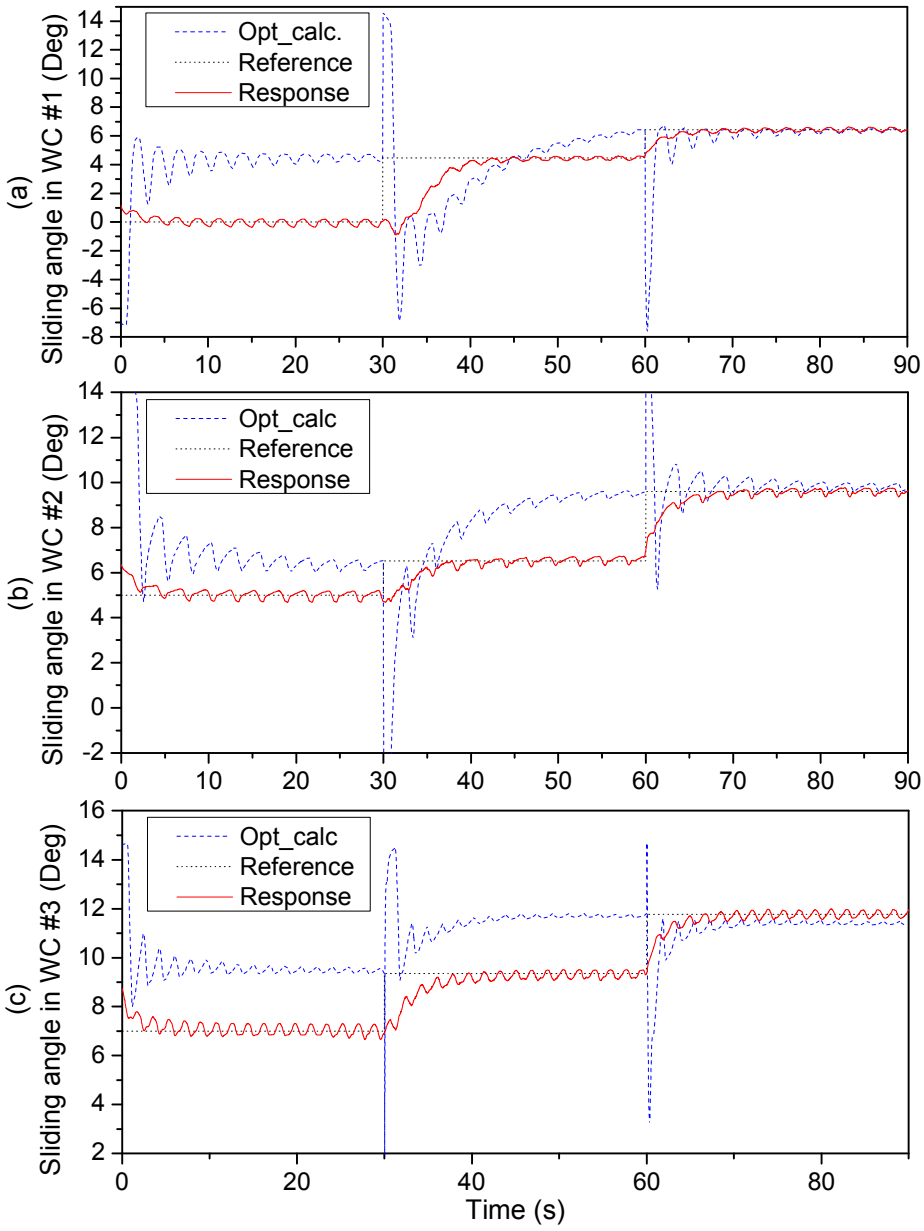

Fig. 12 Sliding angle performance of SAST-WEC in the three wave conditions (WC)

To evaluate the effect of SAST-WEC, the experimental result in WC #3 is analyzed, as in the following figures. Fig. 13 presents wave level versus displacement and speed of the buoy. The experiment time is 90s and divided into three segments. The first time segment is from 0s to 30s, the second one is from 30s to 60s, and the third one is from 60s to 90s. The displacement of the buoy becomes longer in the second and the third time segment, when the sliding angle

increases. Therefore, the speed of the buoy increases from the second and the third 30sec. When the sliding angle converges to the optimal sliding angle, the cylinder force also increases.

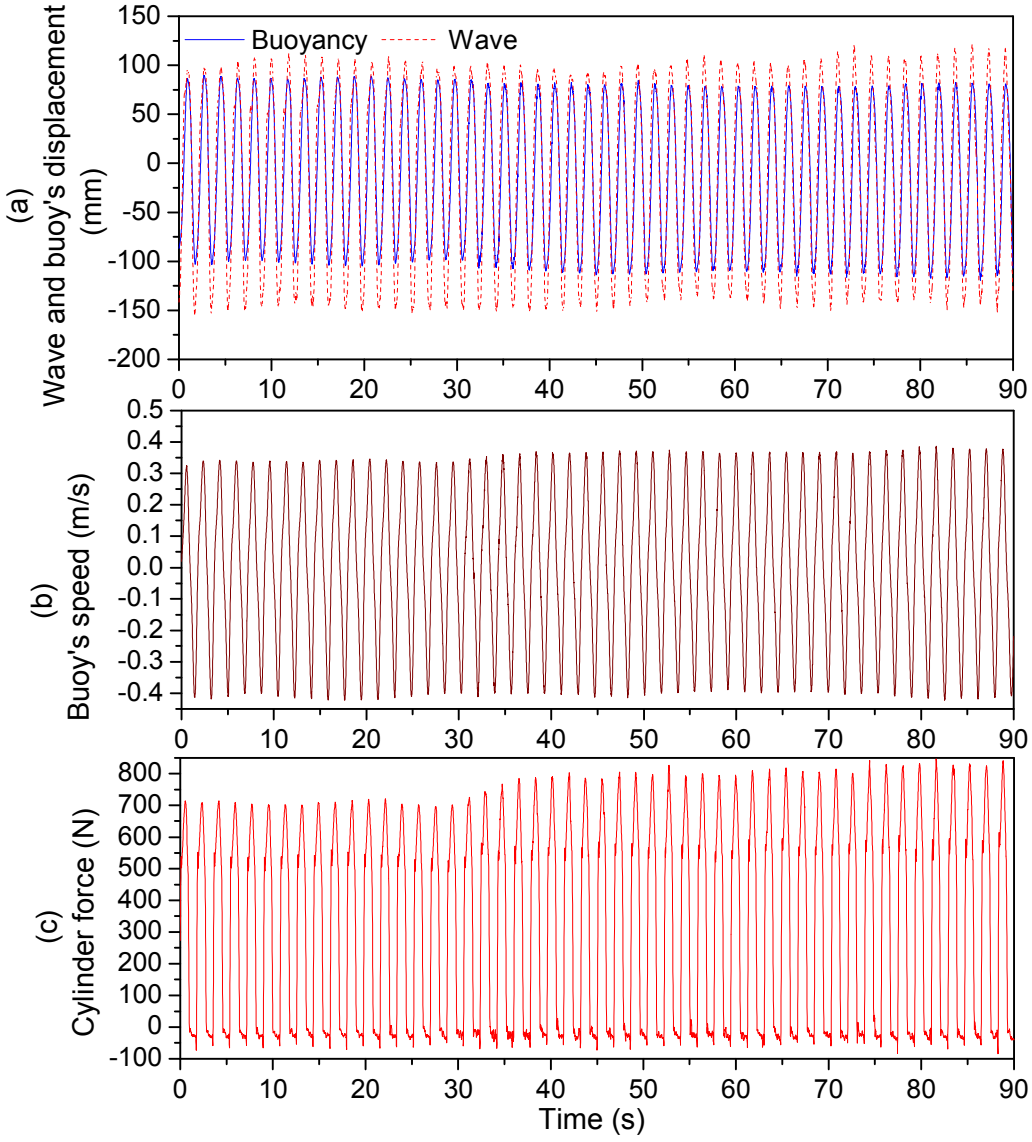

Fig. 13 Wave, displacement of buoy, speed of buoy and cylinder force

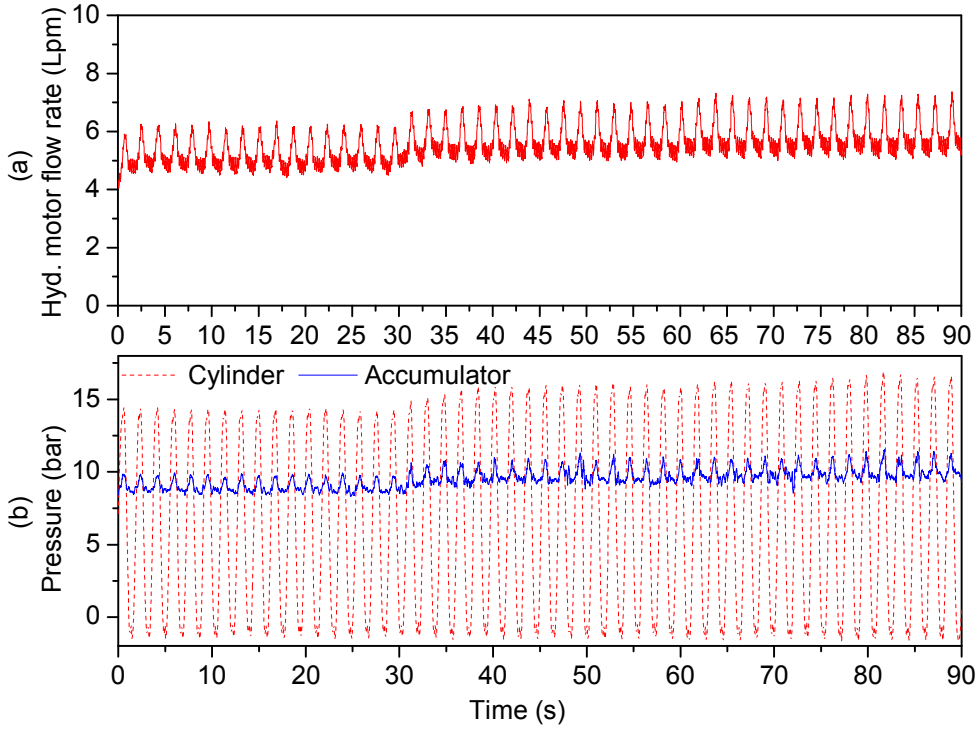

Fig. 14 Flow rate and pressure

The cylinder is operated with a longer displacement, higher speed, and stronger force, so the flow rate of the fluid is supplied to the hydraulic motor and the operating pressure increase as the sliding angle converges to the optimal angle, as shown in Fig. 14. The hydraulic motor supplied the pressurized fluid from the cylinder to drive the 'generator'. For ease of measurement and output torque adjustment, an MR brake is used instead of a real generator. The generator torque and speed, shown in Fig. 15, also increase proportionally to the accumulator pressure and hydraulic motor flow rate, respectively, when the sliding angle tracks the reference sliding angle.

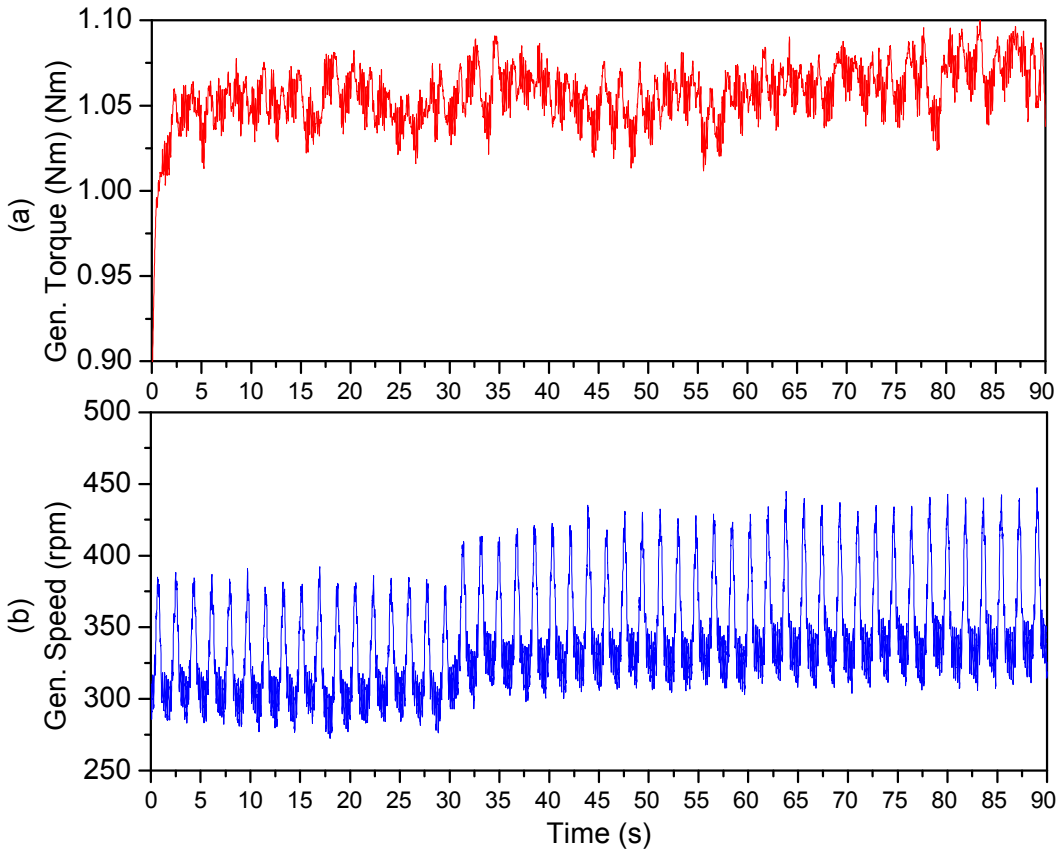

Fig. 15 Torque and speed of the 'generator'

The input power is calculated from the product of the cylinder force and buoyant speed, while the output power is calculated from the product of the generator torque and generator speed. In Fig. 16, the input power varies in a wide range, from -10 to 250W, but due to the effect of the HPA, the output power is quite steady around 35W. The integral of the input/output power is then defined as the input/output energy. At the end of the experiment, the input energy measured at the cylinder is 5509J, while the output energy measured at the motor driven shaft is 3405J. The hydraulic efficiency, which is the ratio of output energy to input energy, is calculated as 61.8%. The overall efficiency is the ratio of output energy to wave energy flux in 90s. Based on Table 4, the overall efficiency is calculated as 26.04%.

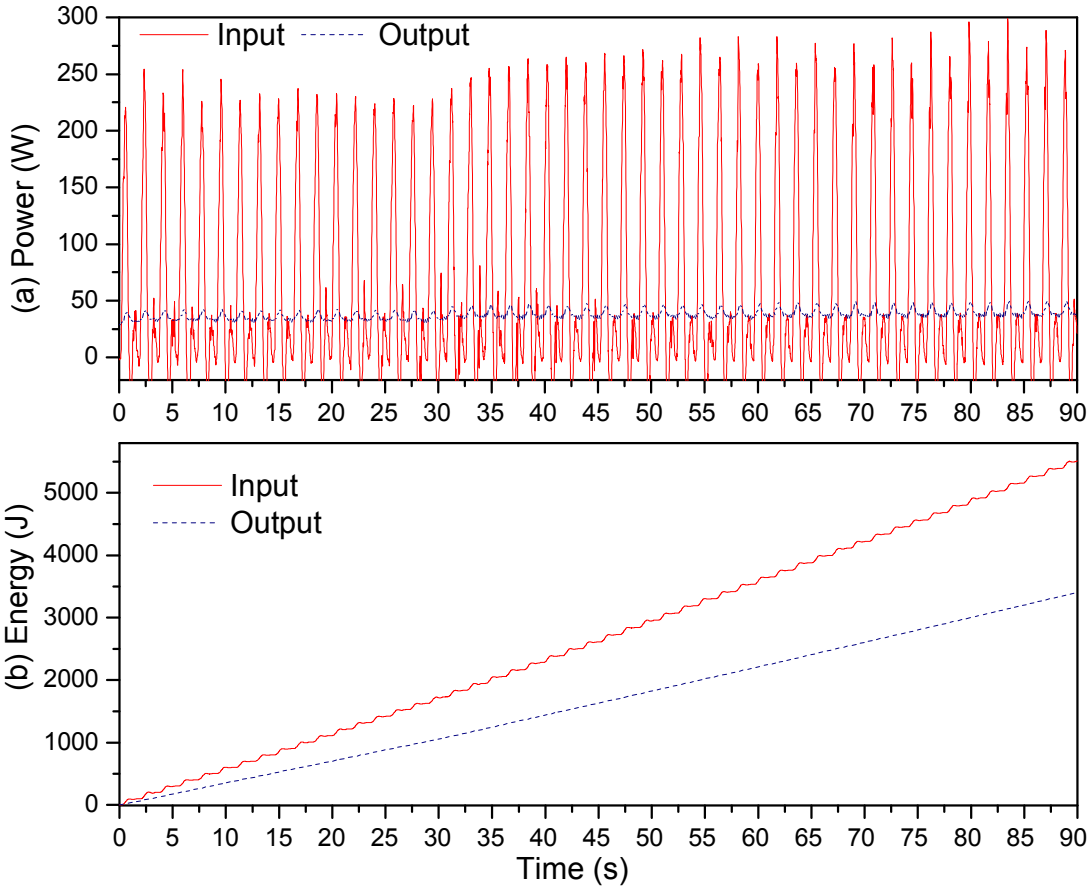

Fig. 16 Input/output power and input/output energy

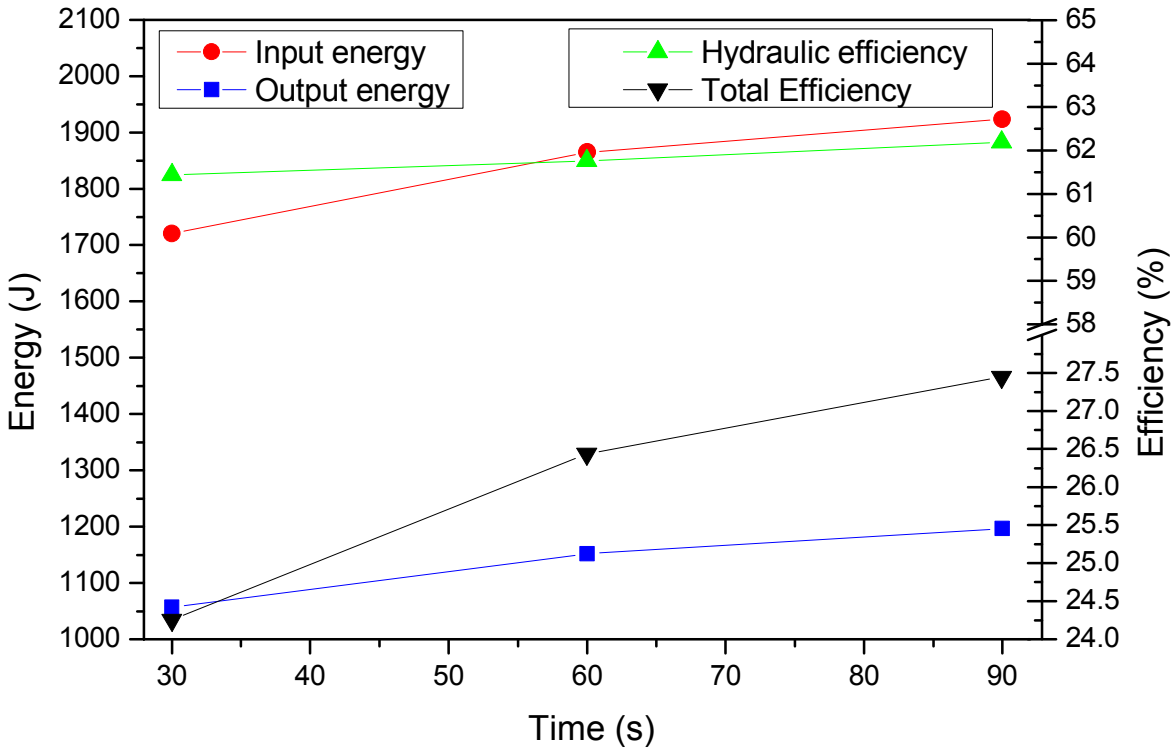

Fig. 17 Input/output energy and efficiencies

The energy data in Fig. 16 are divided into 3 segments: 0-30s, 30-60s and 60-90s. Each 30s of these segment is called the 'angle sampling time'. Fig. 17 shows the evaluation of input/output energy and efficiencies in each 30s of 'angle sampling time'. The circular and square dots display the input and output energy at the end of the angle sampling time: the second 30^{th}, 60^{th}, and 90^{th}, respectively. Hydraulic and overall efficiencies, presented by upward and downward triangular dots, are also calculated at these points. The figure shows that the input and output energy increase as the sliding angle converges to the optimal sliding angle. Although the hydraulic efficiency slightly increases, the overall efficiency is enhanced: from 24.25% to 27.45%. That means % is increased comparing to the conventional WEC.

5. Conclusions and future works

An SAST-WEC was proposed in this paper. In the proposed WEC, the optimal sliding angle of the floating buoy can be automatically adjusted to enhance the output power as well as overall efficiency.

Experiments were carried out in three wave conditions to evaluate the sliding angle performance and effect of SAST-WEC. The experimental results showed that the proposed SAST-WEC can converge to an optimal sliding angle, which differs in each wave condition. Typically, the experimental result in wave condition No. 3 indicated that the overall efficiency can be improved from 24.25% in the vertical motion of floating buoy to 27.45% in the optimal sliding angle.

For future works as the next steps of this project, the following issues will be considered: a full-scale multi-point absorber WEC needs to be developed. In addition, pressure coupling principle will be applied to control speed and improve the transmission efficiency. Therefore, a variable displacement hydraulic motor will be employed instead of the fixed displacement motor. The concept of SAST-WEC has been investigated and developed.

Acknowledgment

This work was partly supported by the New & Renewable Energy of the Korea Institute of Energy Technology Evaluation and Planning (KETEP) grant funded by the Korea government Ministry of Trade, Industry and Energy (G031518511) and by the project titled 'R&D center for underwater construction robotics', funded by the Ministry of Oceans and Fisheries (MOF) and Korea Institute of Marine Science & Technology Promotion (KIMST), Korea (PJT200539).

References

[1] Nielsen, G., Andersen, M., Argyriadis, K., Butterfield, S., Fonseca, N., Kuroiwa, T., Boulluec, M.L., Liao, S.J., Turnock, S.R., Waegter, J., 2006. Specialist committee V.4: ocean wind and wave energy utilization. In: Proceedings of the 16th International Ship and Offshore Structures Congress. UK, 165–211.

[2] Henderson, R., 2006. Design, simulation, and testing of a novel hydraulic power take-off system for the pelamis wave energy converter. Renew. Energy 31 (2), 271–283.

[3] Folley, M., Whittaker, T.J.T., 2009. Analysis of the nearshore wave energy resource. Renew. Energy 34, 1709–1715.

[4] Anbarsooz, M., Passandideh-Fard, M., Moghiman, M., 2014. Numerical simulation of a submerged cylindrical wave energy converter. Renew. Energy 64, 132–143.

[5] Oskamp, Jeffrey A., Özkan-Haller, H. Tuba, 2012. Power calculations for a passively tuned point absorber wave energy converter on the Oregon coast. Renew. Energy 45, 72–77.

[6] Zurkinden, A.S., Ferri, F., Beatty, S., Kofoed, J.P., Kramer, M.M., 2014. Non-linear numerical modeling and experimental testing of a point absorber wave energy converter. Ocean Eng. 78, 11–21.

[7] Evans., D.V., 1976. A theory for wave-power absorption by oscillating bodies. J. Fluid Mech. 77, 1–25. http://dx.doi.org/10.1017/S0022112076001109.

[8] Heikkinen, Heidi, Lampinen, Markku J., Böling, Jari, 2013. Analytical study of the interaction between waves and cylindrical wave energy converters oscillating in two modes. Renew. Energy 50, 150–160.

[9] McNatt, J. C., Venugopal, V., Forehand, D., The cylindrical wave field of wave energy converters, International Journal of Marine Energy 3–4 (2013), e26–e39.

[10] Folley, M., Whittaker, T.J.T., 2009. Analysis of the nearshore wave energy resource. Renew. Energy 34, 1709–1715.

[11] Do, H. T., Dinh, Q. T., Nguyen, M. T., Phan, C. B., Dang, T. D., Lee, S.Y., Park, H. G., Ahn, K. K., 2015, Effects of non-vertical linear motions of a hemispherical-float wave energy converter, Ocean Engineering 109, 430–438.

[12] Anbarsooz, M., Passandideh-Fard, M., Moghiman, M., 2013. Fully nonlinear viscous wave generation in numerical wave tanks. Ocean Eng. 59, 73–85.

[13] Goggins, J., Finnegan, W., 2013, Shape optimisation of floating wave energy converters for a specified wave energy spectrum, Renewable Energy 71, 208-220.

[14] Alves, J.H.G.M., Banner, M.L., Young, I.R., 2003. Revisiting the Pierson–Moskowitz asymptotic limits for fully developed wind waves. J. Phys. Oceanogr. 33, 1301–1323.

[15] Hansen, R.H., Andersen, T.O., Pedersen, H.C., 2011. Model based design of efficient power take-off systems for wave energy converters. In: Proceedings of the 12th Scandinavian International Conference on Fluid Power. Finland.

[16] Ketabdari M.J, Ranginkaman A., 2009, Simulation of Random Irregular Sea Waves for Numerical and Physical Models Using Digital Filters. Transaction B: Mechanical Engineering; 16 (3): 240-247.

[17] Falnes, J., 2002. Ocean Waves and Oscillating Systems. Cambridge University Press, Cambridge, UK.

[18] Cargo, C., Plummer, A., Hillis, A., Schlotter, M., 2011. Optimal Design of a Realistic Hydraulic Power Take-off in IrregularWaves. Centre of Power Transmission and Motion Control-University of Bath, UK.

[19] Rabie, M.G., 2009. Fluid Power Engineering. McGraw-Hill.

[20] Pinches, M.J., Ashby, J.G., 1988. Power Hydraulics. Prentice-Hall, Englewood Cliffs, NJ, USA..

[21] Ho, T.H., Ahn, K.K., 2010. Modeling and simulation of a hydrostatic transmission system with energy recuperation using a hydraulic accumulator. JMST 24 (5), 1163–1175.

[22] McCormick, Michael E., 2010. Ocean Engineering Mechanics with Applications. Cambridge University Press, UK.